



HAL
open science

Monitoring subcutaneous tumors using Mueller polarimetry: study on two types of tumors

Briseis Varin, Jean Rehbinder, Jean Dellinger, Christian Heinrich, Marc Torzynski, Caroline Spenle, Dominique Bagnard, Jihad Zallat

► To cite this version:

Briseis Varin, Jean Rehbinder, Jean Dellinger, Christian Heinrich, Marc Torzynski, et al.. Monitoring subcutaneous tumors using Mueller polarimetry: study on two types of tumors. *Biomedical optics express*, 2021, 12 (10), pp.6055-6065. 10.1364/BOE.433754 . hal-03402871

HAL Id: hal-03402871

<https://hal.science/hal-03402871v1>

Submitted on 7 Dec 2021

HAL is a multi-disciplinary open access archive for the deposit and dissemination of scientific research documents, whether they are published or not. The documents may come from teaching and research institutions in France or abroad, or from public or private research centers.

L'archive ouverte pluridisciplinaire **HAL**, est destinée au dépôt et à la diffusion de documents scientifiques de niveau recherche, publiés ou non, émanant des établissements d'enseignement et de recherche français ou étrangers, des laboratoires publics ou privés.



Monitoring subcutaneous tumors using Mueller polarimetry: study on two types of tumors

BRISÉIS VARIN,¹  JEAN REHBINDER,¹  JEAN DELLINGER,¹
CHRISTIAN HEINRICH,¹  MARC TORZYNSKI,¹ CAROLINE SPENLÉ,²
DOMINIQUE BAGNARD,² AND JIHAD ZALLAT^{1,*}

¹ICube Laboratory, University of Strasbourg, Bd Sébastien Brant, 67412–Illkirch, France

²INSERM U1119–Labex Medalis, University of Strasbourg, Bd Sébastien Brant, 67412–Illkirch, France
*jihad.zallat@unistra.fr

Abstract: A better understanding of tumor development is crucial for treating cancer. Polarimetric imaging is an interesting alternative for monitoring subcutaneous tumors as it is non-invasive. In this study, a Mueller spectro-polarimeter is used to monitor tumor development on mice injected with non-pigmented breast cancer cells or with pigmented murine melanoma cells. Three stages of non-pigmented tumor development are revealed with three polarimetric parameters. These stages also appear for pigmented tumors, although less clearly. A halo of high depolarization surrounding the non-pigmented tumor in the first stage allows the outlining of the tumor. Considering polarimetric parameters, a biological interpretation is proposed.

© 2021 Optical Society of America under the terms of the [OSA Open Access Publishing Agreement](#)

1. Introduction

With an estimated 12.7 million new cases a year [1], cancer is a disease that can affect all populations, regardless of sex and age. However, it is still not perfectly understood, and a better understanding of tumor development could lead to an improvement in treatment. To deepen the knowledge on cancer and its development, many studies first take place on small animals, such as mice.

Decades of research have uncovered a range of complex mechanisms allowing the emergence, growth and spread of tumors. Cancer development involves many biological parameters (genetic, environmental, interactions with the microenvironment, etc.) that cannot be reproduced *ex-vivo*. Mouse models are an ideal platform to improve our understanding of cancers and to develop new drugs [2]: mice are genetically very close to humans and display a great physiological similarity. Their small size, high fecundity and relatively low production and maintenance costs make them an animal of choice for laboratories. In addition, the development of numerous inbred strains has made it possible to obtain batches of genetically very similar animals, thus facilitating comparative studies. While mouse tumor models continue being developed for an ever increasing similarity to human tumors [3,4], simpler subcutaneous implantation of cell-derived xenografts are still frequently used for assessment and validation of new drugs [5]. In this approach, cancerous cells are injected under the skin of immunodeficient mice. Tumor growth is then monitored and compared for mice receiving the treatment under investigation and mice without treatment (or with a standard treatment).

The most common parameter used to do so is tumor volume, measured with a caliper. The measurement of most relevant biological parameters is then only possible through necropsy and time-consuming biochemical and histological analysis of collected samples. In addition to its low information content, tumor volume measurement is also limited to palpable tumors (leaving early proliferation phases inaccessible) and is operator dependent. Finding a method to better monitor tumor development, without having to sacrifice and biopsy the animals will help understand tumor detection, the stage at which the tumor is detected and how to treat that tumor in humans.

To fulfill this need, several non-invasive imaging techniques are currently used for *in-vivo* tumor growth monitoring. Those include positron emission tomography (PET), magnetic resonance imaging (MRI), bioluminescence imaging (BLI), fluorescence imaging (FLI) and ultrasound (US) [6,7]. Here, we propose polarimetric imaging as a non-invasive tool able to detect subcutaneous tumors and monitor their development. This tool would aid the biologists in their cancer studies on small animals.

Polarimetric imaging is promising for several reasons. First, it has been shown that biological tissues modify the polarization of light [8]: the structure of cells and fibers affect the depolarization of the backscattered light, whereas collagen fibers for example contribute to birefringence effects. Different types of tissues will have different polarimetric responses. This method is also non-invasive and has a wide field of view. Several studies have demonstrated the potential of this technique to characterize cancerous regions for a variety of tissues: colon, intestine, rectum, skin and cervix [9–13]. In comparison with other *in-vivo* tumor growth monitoring techniques, polarimetric imaging does not require any staining or special preparation of the animals and can be performed rapidly for large studies.

In this study, a Mueller spectro-polarimeter has been developed to allow polarimetric imaging of skin. The prototype is non-temperature dependent and calibration-free [14]. It can image small animals as well as humans. In a previous study, the prototype was used on several mice, and showed pigmented-tumor development impacted depolarization [15]. Here, a biological study involving several mice is implemented to allow tumor development monitoring with the Mueller spectro-polarimeter. Each mouse is injected with one of two types of cancer cells under the skin and is imaged twice a week. Several parameters derived from the measured Mueller matrix are examined to quantify tumor development.

The paper is structured as follows: Sec. 2 describes the instrument and method used in this study, as well as the organization of the biological study. Sec. 3 presents the results of the study concerning the monitoring of tumor development for two types of tumors, as well as a method to outline the tumor. In Sec. 4, our work is summarized and conclusions are drawn.

2. Methods

2.1. Mueller spectro-polarimeter

The imaging system used in this study is a home-built Mueller spectro-polarimeter, whose architecture is represented on Fig. (1(b)). The sample is illuminated by four LEDs at different wavelengths (Thorlabs, M680F3, M740F2, M810F2 and M880F2). The prototype used in this study illuminates in the near-IR at 680 nm, 740 nm, 810 nm and 880 nm. The light provided by the LED is modulated when passing through the polarization state generator (PSG), composed of a linear polarizer followed by two differential liquid crystal modulators. Each differential modulator consists in two liquid crystal variable retarders (LCVR, Meadowlark, custom mount) with their fast axis placed at 90° from one another. This structure helps get rid of the temperature dependence common with LCVRs [14]. Light backscattered on the sample passes through the polarization state analyzer (PSA), constituted of the same elements as the PSG placed in reverse order. Finally, the image produced is captured by a CCD camera (Stemmer Imaging, Allied vision Manta). The optical setup is encased in an opaque hand-held medical plastic case. Imaging is performed through a glass window at the bottom of the prototype.

The PSG and PSA are calibrated using double-pass spectral calibration [16,17]. The system as a whole is calibrated using the Eigen-values Calibration method, described in Ref. [18]. Once it has been calibrated, the spectro-polarimeter acquires, at each wavelength, sixteen images for sixteen different polarimetric states induced by the PSG and the PSA. The Mueller matrix of the sample at wavelength λ is then calculated from those sixteen images and calibration data:

$$M^\lambda = [M_{i,j}^\lambda]_{i,j \in [1,4]} \quad (1)$$

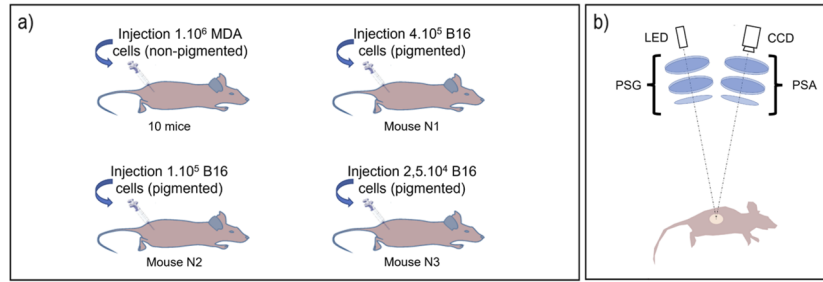


Fig. 1. (a) Schematic representation of the study organization. Several nude mice are injected with non-pigmented or pigmented tumor cells, at different concentrations. (b) Schematic representation of the Mueller spectro-polarimeter. The system is illuminated with LEDs. The light goes through a Polarization State Generator, is reflected on the skin of the mouse. Then the light goes through a Polarization State Analyzer before the image is captured by a CCD camera.

In the following, we analyze the evolution of either simple linear combinations of Mueller matrix elements or of elementary polarimetric parameters extracted using the Lu-Chipman decomposition [19,20]. With this method, the Mueller matrix of the sample is written as the product of three matrices:

$$M = M_{\Delta} M_R M_D \quad (2)$$

where M_{Δ} , M_R and M_D are respectively the Mueller matrices of a depolarizer, a retarder and a diattenuator. With this decomposition, the depolarization, retardance and diattenuation can be determined.

From Eq. (1) and Eq. (2), three polarimetric parameters are used in this study. First, the difference between the first and last elements of the Mueller matrix $M_{11}-M_{44}$ is used as a metric of circular depolarization. The difference $M_{11}-M_{44}$ is similar to the results obtained with crossed circular incident and reflected polarized states. The circular dichroism can be neglected. This parameter eliminates efficiently the effects of specular reflection. The range of this parameter corresponds to the range of the intensity images, in our case the values provided by the camera. Then, the depolarization obtained with the Lu-Chipman decomposition from Eq. (3) is used to determine the spectral difference Δ_{Depol} :

$$\Delta = 1 - \frac{|tr(M_{\Delta}) - 1|}{3}, 0 \leq \Delta \leq 1 \quad (3)$$

$$\Delta_{Depol} = \Delta_{880} - \Delta_{680} \quad (4)$$

We use discrete spectral measurements to capture significant parameters useful for early detection and monitoring of tumors. Our measurements show that the spectral difference of the depolarization parameter is important.

Finally, the orientation of the retarder α can be determined from the retardance R :

$$\alpha = \frac{1}{2} \arctan\left(\frac{a_2}{a_1}\right), 0 \leq \alpha \leq 2\pi \quad (5)$$

With

$$\forall i \in \{2, 3, 4\}, a_i = \frac{1}{2 \sin(R)} \sum_{j,k=2}^4 \varepsilon_{ijk}(m_R)_{jk} \quad (6)$$

And

$$R = \arccos\left(\frac{tr(m_R) - 1}{2}\right), 0 \leq R \leq \pi. \quad (7)$$

2.2. Study organization

Monitoring of tumor growth *in-vivo* with the Mueller spectro-polarimeter is demonstrated by inducing tumor growth in mice.

A total number of ten mice are initially included in this study. The animals are Nude mice SOPF ATHYMIC NUDE FEM 8 S/ CrI:NU(NCr)-Foxn1 <nu> (Charles Rivers), a strain frequently used for the study of grafted human tumors. They are characterized by an inhibited immune system and a lack of fur. The mice are injected with 1.10^6 MDA-MB231 cells (sigma), a human breast cancer cell line used in breast cancer research for its highly metastatic potential. The injections are subcutaneous, i.e., under the skin, and are realized at the top of the left thigh. They result after a few days in the development of subcutaneous, non-pigmented tumors. At the beginning of the study, four tattoo points are added around the injection site, to help monitor the polarimetric response. The mice are included in the study analysis once tumor development is confirmed. We refer to the day the mice are included in the study as “day of inclusion”. The inclusion of a mouse in the study occurs once the tumor volume has reached a threshold of 20mm^3 . The day of inclusion varies from one mouse to the other.

In parallel, three other Nude mice are injected with B16 melanoma cells, a murine tumor cell line used for research as a model for skin cancers. Each mouse is injected with a different quantity of cells: mouse N1 receives 4.10^5 cells, mouse N2 receives 1.10^5 cells and mouse N3 receives $2,5.10^4$. The injections lead to the development of pigmented tumors under the skin. Four tattoo points are also added around the injection site at the beginning of the study. A schematic representation of all the mice part of this work and their injections can be found in Fig. (1(a)). The main difference between this type of tumor and the one resulting from the injection of breast cancer cells is the pigmentation. The melanoma tumor will be easily visible and trackable with the naked eye, whereas the breast cancer tumor will be more difficult to measure and will cause little to no visible change on the surface of the tissue at the beginning of tumor development.

The two tumor cell types will have different growth dynamics, and their tumor growth may vary in some ways. The comparison of polarimetric responses during tumor growth will help tell if some polarimetric responses seen in tumor growth are common to a range of different crafted tumors.

Tumor growth is monitored twice a week from the day of injection until the sacrifice. This is realized by estimating tumor volume using the standard caliper measurements and by polarimetric imaging using our system in parallel. Before both procedures, the mice are put under anesthesia by inhalation of isoflurane. After examination by palpation, the length (L) and width (l) of identified tumors is measured using caliper. The volume of the tumor (V) is estimated using the approximate ellipsoid formula:

$$V = \frac{L \times l^2}{2} \quad (8)$$

For polarimetric imaging, mice are placed on a custom-built holder ensuring isoflurane supply and stability during measurement. Positioning of the polarimeter is carried out by including the four reference tattoo points in the image and pressing the imaging window against the skin of the mouse. The experiment on small animals was authorized by Apafis #14058 2018031317278197.

Throughout the rest of this paper, the timestamps of the study shall be named “d + number of days since the injection”. For example, “d16” will refer to the measurement taken 16 days after tumor cells were injected.

3. Results and discussion

Tumor growth for pigmented and non-pigmented tumors was imaged with the spectro-polarimeter developed in this study following the protocol described in the previous section. In the following section, the evolution of several polarimetric parameters is analyzed throughout tumor

development, first for non-pigmented tumors, then for pigmented tumors. The analysis reveals different parameters are sensitive to the tumor at different stages of its development. Additionally, one parameter helps detect the outline of the tumor in the early stages of its development for non-pigmented tumors.

3.1. Stages of tumor development for non-pigmented tumors

The evolution of normalized mean tumor volume for the mice injected with breast cancer cells is shown in Fig. (2). If no palpable tumor is detected, the volume is set to 0. An important and expected tumor growth can be seen for these mice.

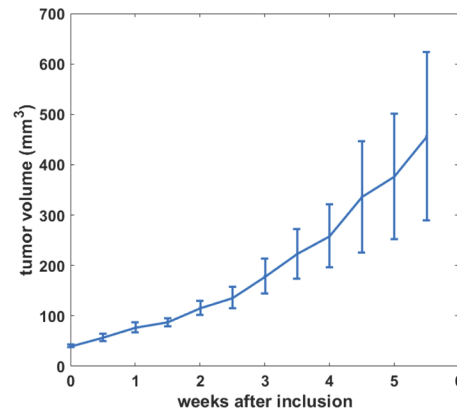


Fig. 2. . Evolution of tumor volume in time. Tumor volumes for the ten mice are represented depending on the number of weeks after the mice were included in the analysis. The errorbars correspond to the Standard Error of the Mean.

Tumor development is monitored using the measurements realized with the spectro-polarimeter. Throughout the study, we observed healthy mouse skin to have a high depolarization ratio, almost no retardance signal nor diattenuation. There is little to no spectral dependence of the polarimetric parameters in the covered spectral range. This is interpreted as being due to the high scattering coefficient of skin [21]. During tumor development, we have identified three polarimetric signatures of the tumor appearing sequentially. We illustrate these contrasts with one representative mice of the study, as shown in Fig. (3(a)). As seen with tumor volume, mice go through full development of injected tumors.

Evolution of polarimetric parameters A prior study [15] had shown that the development of a tumor is accompanied with a drop in depolarization. In this study, we also observe that early tumor development is accompanied by a drop of depolarization in the region of the tumor. In Fig. (3(a)), we use the difference $M_{11}-M_{44}$ as a metric for depolarization (second line). Before tumor cells are injected, at d1, when the skin imaged is healthy, it presents a uniformly high value of depolarization. Then, it can be noted that the tumor is clearly visible with depolarization at the beginning of the study (at d16): the tumor has a lower depolarization than healthy skin. However, in the middle of the study when the tumor has become larger ($\sim 150\text{mm}^3$ in this case), the depolarization value for the tumor area becomes higher than at the beginning of the study. It presents values similar to the healthy skin around, and the tumor becomes less clearly visible with the depolarization. This continues until the end of the study, with the exception of necrotic tissues. The necrotic tissues are visible with depolarization since they are very dark and pigmented.

As the depolarization becomes less affected by the tumor, another polarimetric indicator starts to show variations on the injection site. It is the spectral difference Δ_{Depol} between the depolarization measured at 680 nm and the depolarization measured at 880 nm. The third line

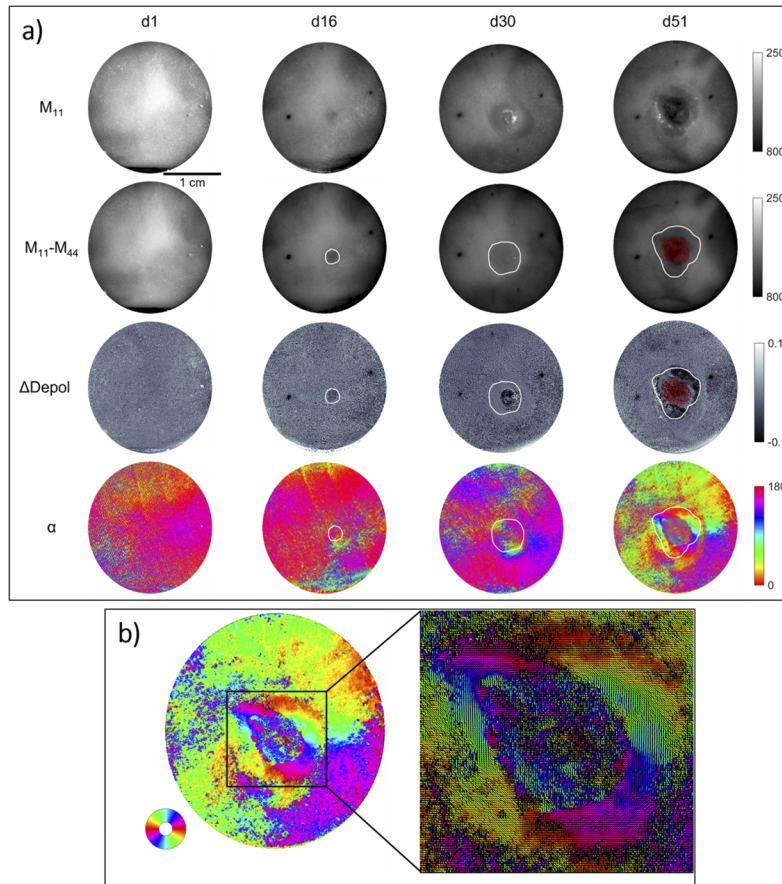


Fig. 3. a) Evolution of three polarimetric parameters during the study for a mouse injected with breast cancer cells. The four columns correspond to four timestamps of the study: d1 on the first day of the study, before the injection of tumor cells, d16 at the beginning of the study, d30 at the mid-point of the study and d51 is the day the mouse is sacrificed. On the first line, the M_{11} images for those four timestamps are provided, showing the aspect of the tumor. On the second line, depolarization for those four timestamps is given. The third line provides the images of the spectral difference Δ_{Depol} of depolarization. The fourth line corresponds to the images of the orientation of the retarder α . The tumor has been outlined in white on each figure. The red area seen in the images for d51 correspond to necrotic tissues. b) The orientation of the retarder α for d51 is shown, with a zoom on the tumor [22].

of Fig. (3(a)) provides images of this parameter before the injection of tumor cells, and at the beginning, middle and end of the study. When the tissue is healthy, at d1, this parameter equals zero. However, it appears that the tumor is clearly visible at the middle of the study, once the tumor has become larger: the spectral difference Δ_{Depol} is five times bigger for the tumor than it is for healthy skin around the tumor. Moreover, with this parameter the outline of the tumor appears neatly, which makes the detection of the tumor easier. At the end of the study, when the tumor becomes necrotic, it becomes less apparent with the spectral difference Δ_{Depol} . Although the polarimetric parameter is still impacted, the center of the tumor has a lower spectral difference Δ_{Depol} than in the middle of the study. The delineation of the tumor is also less neatly visible at the end of the study.

A third polarimetric contrast takes over at the end of the study. This parameter, denoted α , is the orientation of the retarder, calculated from M_R introduced in equation Eq. (2), and that can be seen on the last line of Fig. (3(a)). The orientation of the retarder α does not show any pattern at the beginning of the study. When the tissue is healthy, the orientation of the retarder α presents a set value, that can change between areas of the sample. At the middle (d30), a circular pattern begins to appear around the area where spectral difference Δ_{Depol} of depolarization is observed. At the end (d51) it reveals the delineation of the tumor clearly. The inside of the tumor also presents a noticeable signal, quite different from the one of healthy skin. This phenomenon can be observed more precisely on Fig. (3(b)) where the orientation of the retarder α is shown zoomed in on the tumor. The parameter presents a circular variation around the tumor.

Biological interpretation This study has revealed that as the tumor grows, it affects three different polarimetric parameters one after the other. This sequence could be linked to biological phenomena happening during tumor development. The signal observed with depolarization can be related to the disorganization of skin tissue due to the cell cluster that is the tumor. A possible effect is that the tumor pushes away highly scattering fibers while being quite homogenous, thus causing a drop in depolarization. Then, as the tumor grows, it goes deeper in the skin, and can be seen differently with a higher wavelength. That is why the spectral difference Δ_{Depol} shows new information on tumor development. Moreover, this parameter can also be impacted by the fibrosis appearing. At the end of the study, the appearance of necrotic areas in the tumor are probably responsible for the change in polarimetric response: the orientation of the retarder α becomes sensible to those areas, whereas the other polarimetric parameters are not.

3.2. Stages of tumor development for pigmented tumors

Evolution of polarimetric parameters Tumor development for the pigmented tumors is monitored here with polarimetric imaging. Similar to the previous part, depolarization, spectral difference in depolarization Δ_{Depol} and orientation of the retarder α are analyzed. The goal is to determine whether the three stages observed for non-pigmented human breast cancer tumors are also visible for pigmented murine melanomas. The contrasts for these three parameters for the mouse N1 are given in Fig. (4) for three timestamps of the study: d1 corresponds to the day of the injection, d9 at the middle of the study and d18, last time point of the study and day of the sacrifice of the mouse. Tumor development is much faster for murine melanoma than for human breast cancer and the speed of development is proportional to the quantity of cells injected. That is why the mouse N1 is sacrificed so early.

A first clear difference with tumor development for non-pigmented tumors appears with depolarization. For pigmented tumors, the tumor is visible throughout its whole development with depolarization. As the tumor grows, the depolarization drops, and the drop intensifies with time. When looking at the spectral difference in depolarization Δ_{Depol} , the tumor is barely visible at the middle of the study but becomes visible at the end of the study. The response in spectral difference Δ_{Depol} seen for d18 is similar to the response seen at the middle of the study for non-pigmented tumors. Like the development of non-pigmented tumors, the orientation

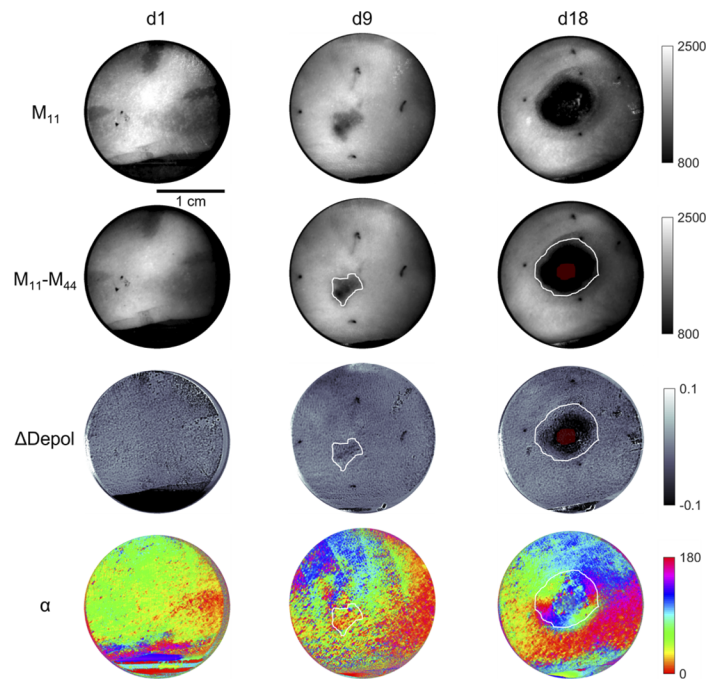


Fig. 4. Evolution of three polarimetric parameters during the study for the mouse N1 in the study. The three columns correspond to three timestamps of the study: d1 at the beginning of the study, d9 at the mid-point of the study and d18 is the day the mouse is sacrificed. On the first line, the M_{11} images for those three timestamps are provided, showing the aspect of the tumor. On the second line, depolarization for those three timestamps is given. The second line provides the images of the spectral difference of depolarization Δ_{Depol} . The third line corresponds to the images of the orientation of the retarder α . The tumor has been outlined in white on each figure. The red area seen in the images on d18 correspond to necrotic tissues.

of the retarder α for pigmented tumors is only impacted by the tumor at the end of the study. However, the outline of the pigmented tumor is less neatly visible than for non-pigmented tumors. Thus, although the three parameters defined in the previous part are all impacted by the tumor development, the three stages of development are not as distinct as for the non-pigmented tumors. The impact on each parameter does also not appear sequentially, unlike for non-pigmented tumors.

Biological interpretation The origin of these differences is still uncertain. It is known that the pigmentation of the tumor leads to an increase in absorption. The absorption in turn impacts the depolarization. These differences in absorption can explain why the pigmented tumor is visible with depolarization throughout the whole study, unlike for non-pigmented tumors. The pigmented tumors resulting from the injections of murine melanoma cells also developed much faster than the non-pigmented tumors. Depending on the number of cells injected, the tumors reached necrosis in between 18 and 35 days, whereas tumor development lasted twice as long for some of the mice injected with breast cancer cells. The proliferation of melanoma cells can be monitored with depolarization, thanks to the pigmentation of the cells. The cell proliferation may be so fast that the tumor reaches the volume at which the mouse needs to be sacrificed before the structure of the tissues around it have time to change. Since the last two stages of tumor development observe for non-pigmented tumors are linked to structural changes in the tissue, the

fast cell proliferation may explain why the two last stages of tumor development appear so late in the study.

3.3. Outlining the breast cancer tumor in its first stage

When examining non-pigmented tumor development, a particular phenomenon can be observed during the first stage. As said earlier, tumor development in the first stage is linked to a drop in depolarization. However, it can also be noticed that the tumor is surrounded by an area with a higher depolarization. This can be observed in Fig. (5), where the intensity image and corresponding depolarization are visible for two timestamps of the study for a mouse injected with breast cancer cells. The depolarization profile along a line going through the tumor is shown. It can be noticed that healthy skin has a high depolarization value, between [0.85; 0.9]. On the given depolarization profiles, the drop in depolarization for the tumor is clearly visible: the depolarization goes down to less than 0.8. Around the tumor, a white area which we called a halo can be observed. In Fig. (5) this phenomenon is visible on both depolarization images, but more so on the depolarization image for d27. It is also shown on the depolarization profiles: at d23, the depolarization before and after the drop goes up to 0.93; at d27, it reaches 0.94. With this halo, the tumor can be seen more easily with depolarization, and its outline can be known with greater precision. This phenomenon appears early in the first stage and lasts until the beginning of the second stage.

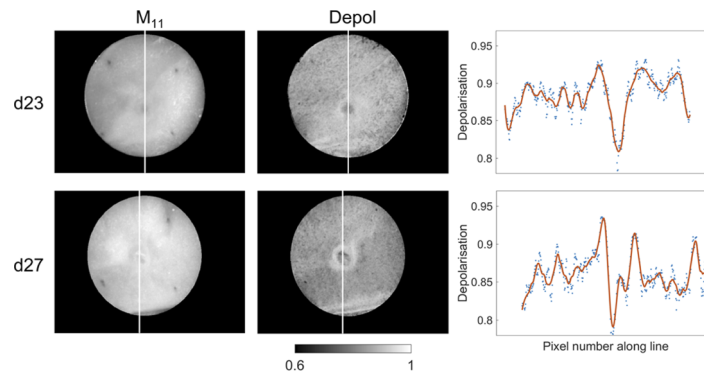


Fig. 5. Depolarization halo. Evolution of selected parameters between two consecutive measurement days is shown (top row: d23 after injection, bottom row: d27). Each day, M_{11} image (left), depolarization image (center) and a depolarization profile (right) are displayed. The depolarization profile is taken along the white line indicated in the M_{11} image.

Biologically, it can be explained by the pressure applied by the tumor to the surrounding tissue. The appeal of the phenomenon appears for biological studies: it is important for biologists to be able to precisely outline the tumor, especially when it is not visible to the naked eye.

4. Conclusions

In this work, polarimetry has been used to monitor tumor development. A compact and drift-free Mueller spectro-polarimeter has been developed and tested on several mice. Each mouse was injected with either non-pigmented human breast cancer cells or pigmented murine melanoma cells, that developed into tumors right under the skin.

Three stages of tumor development of non-pigmented tumors have been identified with the Mueller spectro-polarimeter, each one spotted with a different polarimetric parameter: depolarization for the first stage, the spectral difference of depolarization Δ_{Depol} for the second stage, and the orientation of the retarder α for the final stage. Each stage is linked to a biological

phenomenon. In the first stage, when the tumor is not yet, or not easily visible to the naked eye, a phenomenon has been detected to precisely outline the tumor: the drop in depolarization linked to the tumor is surrounded by a halo of high depolarization. For pigmented tumors, depolarization is impacted by the tumor throughout the whole study. The two following stages of development are not as clearly visible as for non-pigmented tumors: pigmented tumors are only detected with spectral difference in depolarization Δ_{Depol} and with the orientation of the retarder α at the end of the study. The instrument presented here offers a new method to monitor tumor development, that provides more information than the traditional methods (tumor volume. . .) do. The biological stage of the development can be known without having to biopsy the tumor and sacrifice the animal.

This study has shown that polarimetric imaging provides more information on tumor monitoring than the standard biological parameters (i.e., tumor volume). The Mueller spectro-polarimeter used is noninvasive: it is a promising tool for the monitoring of tumor development for biological studies.

Funding. Société d'Accélération du Transfert de Technologies Conectus Alsace (Dermapol project).

Acknowledgments. The authors are grateful to the anonymous reviewers for their very useful comments that helped to make better the manuscript. The authors would like to thank Jordan Schmidt for his help with sample preparation and acquiring data.

Disclosures. The author declares non conflict of interest.

Data availability. Data underlying the results presented in this paper are not publicly available at this time but may be obtained from the authors upon reasonable request.

References

1. J. Ferlay, H. R. Shin, F. Bray, D. Forman, C. Mathers, and D. M. Parkin, "Estimates of worldwide burden of cancer in 2008: GLOBOCAN 2008," *Int. J. Cancer* **127**(12), 2893–2917 (2010).
2. C. P. Day, G. Merlino, and T. Van Dyke, "Preclinical mouse cancer models: a maze of opportunities and challenges," *Cell* **163**(1), 39–53 (2015).
3. G. Dranoff, "Experimental mouse tumour models: What can be learnt about human cancer immunology?" *Nat. Rev. Immunol.* **12**(1), 61–66 (2012).
4. M. Landgraf, J. A. McGovern, P. Friedl, and D. W. Hutmacher, "Rational design of mouse models for cancer research," *Trends Biotechnol.* **36**(3), 242–251 (2018).
5. J. Jung, "Human tumor xenograft models for preclinical assessment of anticancer drug development," *Toxicol. Res.* **30**(1), 1–5 (2014).
6. S. K. Lyons, "Advances in imaging mouse tumour models in vivo," *J. Pathol.* **205**(2), 194–205 (2005).
7. A.-L. Puaux, L. C. Ong, Y. Jin, I. Teh, M. Hong, P. K. H. Chow, X. Golay, and J.-P. Abastado, "A comparison of imaging techniques to monitor tumor growth and cancer progression in living animals," *Int. J. Mol. Imaging* **2011**, 1–12 (2011).
8. N. Ghosh and A. I. Vitkin, "Tissue polarimetry: concepts, challenges, applications, and outlook," *J Biomed Opt* **16**(11), 110801 (2011).
9. M.-R. Antonelli, A. Pierangelo, T. Novikova, P. Validire, A. Benali, B. Gayet, and A. De Martino, "Mueller matrix imaging of human colon tissue for cancer diagnostics: how Monte Carlo modeling can help in the interpretation of experimental data," *Opt. Express* **18**(10), 10200 (2010).
10. W. Wang, L. G. Lim, S. Srivastava, J. Bok-Yan So, A. Shabbir, and Q. Liu, "Investigation on the potential of Mueller matrix imaging for digital staining," *J. Biophotonics* **9**(4), 364–375 (2016).
11. A. Pierangelo, S. Manhas, A. Benali, C. Fallet, J.-L. Totobenazara, M.-R. Antonelli, T. Novikova, B. Gayet, A. De Martino, and P. Validire, "Multispectral Mueller polarimetric imaging detecting residual cancer and cancer regression after neoadjuvant treatment for colorectal carcinomas," *J. Biomed. Opt.* **18**(4), 046014 (2013).
12. S. L. Jacques, J. R. Roman, and K. Lee, "Imaging superficial tissues with polarized light," *Lasers Surg. Med.* **26**(2), 119–129 (2000).
13. A. Pierangelo, A. Nazac, A. Benali, P. Validire, H. Cohen, T. Novikova, B. H. Ibrahim, S. Manhas, C. Fallet, M.-R. Antonelli, and A.-D. Martino, "Polarimetric imaging of uterine cervix: a case study," *Opt. Express* **21**(12), 14120 (2013).
14. B. Varin, J. Dellinger, J. Rehbinder, C. Draman, M. P. Torzynski, C. Heinrich, and J. Zallat, "Ultra-stable spectropolarimeter for dermatology," in *Advanced Biomedical and Clinical Diagnostic and Surgical Guidance Systems XVIII* A. Mahadevan-Jansen, ed. (SPIE, 2020), Vol. 11229, p. 26.
15. B. Varin, J. Rehbinder, J. Dellinger, C. Heinrich, J. Schmidt, C. Spenlé, D. Bagnard, and J. Zallat, "Tumor growth monitoring using polarized light," in *Novel Biophotonics Techniques and Applications V*, A. Amelink and S. K. Nadkarni, eds. (SPIE, 2019), p. 27.

16. J. Zallat, M. Torzynski, and A. Lallement, "Double-pass self-spectral-calibration of a polarization state analyzer," *Opt. Lett.* **37**(3), 401 (2012).
17. D. Layden, M. F. G. Wood, and I. A. Vitkin, "Optimum selection of input polarization states in determining the sample Mueller matrix: a dual photoelastic polarimeter approach," *Opt. Express* **20**(18), 20466–20481 (2012).
18. E. Compain, S. Poirier, and B. Drevillon, "General and self-consistent method for the calibration of polarization modulators, polarimeters, and Mueller-matrix ellipsometers," *Appl. Opt.* **38**(16), 3490 (1999).
19. S.-Y. Lu and R. A. Chipman, "Interpretation of Mueller matrices based on polar decomposition," *J. Opt. Soc. Am. A* **13**(5), 1106 (1996).
20. C. Heinrich, J. Rehlinger, and J. Zallat, "Revisiting the generalized polar decomposition of Mueller matrices," *J. Opt. Soc. Am. A* **37**(8), 1327–1339 (2020).
21. S. L. Jacques, "Optical properties of biological tissues: a review," *Phys. Med. Biol.* **58**(11), R37–R61 (2013).
22. P. Schucht, H.R. Lee, M. Mezouar, E. Hewer, A. Raabe, M. Murek, I. Zubak, J. Goldberg, E. Kovari, A. Pierangelo, and T. Novikova, "Visualization of white matter fiber tracts of brain tissue sections with wide-field imaging Mueller polarimetry," *IEEE Trans. Med. Imaging* **39**(12), 4376–4382 (2020).